Plant Soil (2010) 328:291–302
DOI 10.1007/s11104-009-0109-8

REGULAR ARTICLE

Analysis of nickel concentration profiles around the roots of the hyperaccumulator plant *Berkheya coddii* using MRI and numerical simulations

A. B. Moradi · S. E. Oswald · J. A. Nordmeyer-Massner · K. P. Pruessmann · B. H. Robinson · R. Schulin

Received: 8 April 2009 / Accepted: 11 July 2009 / Published online: 25 July 2009

Abstract Investigations of soil-root interactions are hampered by the difficult experimental accessibility of the rhizosphere. Here we show the potential of Magnetic Resonance Imaging (MRI) as a non-destructive measurement technique in combination with numerical modelling to study the dynamics of the spatial distribution of dissolved nickel (Ni^{2+}) around the roots of the nickel hyperaccumulator plant *Berkheya coddii*. Special rhizoboxes were used in which a root monolayer had been grown, separated from an adjacent inert glass bead packing by a nylon membrane. After applying a Ni^{2+} solution of 10 mg l^{-1}, the rhizobox was imaged repeatedly using MRI. The obtained temporal sequence of 2-dimensional Ni^{2+} maps in the vicinity of the roots showed that Ni^{2+} concentrations increased towards the root plane, revealing an accumulation pattern. Numerical modelling supported the Ni^{2+} distributions to result from advective water flow towards the root plane, driven by transpiration, and diffusion of Ni^{2+} tending to eliminate the concentration gradient. With the model, we could study how the accumulation pattern of Ni^{2+} in the root zone transforms into a depletion pattern depending on transpiration rate, solute uptake rate, and Ni^{2+} concentration in solution.

Keywords *Berkheya coddii* · Concentration gradient · Hyperaccumulator · Magnetic resonance imaging · MIN3P · Modelling · Nickel · Uptake

Responsible Editor: Henk Schat.

A. B. Moradi (✉) · B. H. Robinson · R. Schulin
Soil Protection group, Institute of Terrestrial Ecosystems,
ETH Zurich,
CHN F28.2, Universitaetstrasse 16,
CH-8092 Zurich, Switzerland
e-mail: ahmad.moradi@env.ethz.ch

S. E. Oswald
Hydrogeology Department, Helmholtz Centre
for Environmental Research—UFZ,
Permoserstraße 15,
04318 Leipzig, Germany

J. A. Nordmeyer-Massner · K. P. Pruessmann
Institute for Biomedical Engineering,
University and ETH Zurich,
Zurich, Switzerland

Present Address:
A. B. Moradi
Hydrogeology Department, Helmholtz Centre
for Environmental Research—UFZ,
Permoserstraße 15,
04318 Leipzig, Germany
e-mail: ahmad.moradi@ufz.de
URL: http://www.ufz.de/index.php?de=17424

Introduction

The focus of rhizosphere studies has recently been opened to the fate of soil pollutants such as heavy metals as a consequence of increasing awareness of soil pollution problems and the attempts to control the pollutants and to remediate contaminated soils

(Wenzel 2005). Nickel is a heavy metal of concern in soil that can be of geogenic origin, as in serpentine soils (Robinson et al. 1999), or may arise from anthropogenic pollution (Brooks 1998; Ashworth and Alloway 2004). Nickel hyperaccumulator plants growing on serpentine soils are able to accumulate at least ten times more nickel than other plant species growing in the same environment (Brooks et al. 1977). Therefore, some hyperaccumulator plants may offer a sustainable treatment option for the remediation of metal-contaminated sites, and an opportunity to mine naturally metal-rich soils by phytomining (Brooks et al. 1998; Li et al. 2003). An attractive plant for phytoextraction of Ni is *Berkheya coddii* Roessler. Its extraordinary phytoextraction potential results from the rare combination of high biomass (22 t ha^{-1}), and high capacity of Ni accumulation in its above-ground biomass which can reach up to 1% w:w (Robinson et al. 1997). Despite this, little is known about the mechanism of Ni hyperaccumulation and root-soil interactions of Ni hyperaccumulator plants including *Berkheya coddii*. Understanding these mechanisms and interactions could help improving methods for the phytoextraction of Ni from contaminated soils and also phytomining (McNear et al. 2005).

However, investigating root-soil interactions such as the uptake of metals by roots is challenging. It requires a high-resolution data on the spatial distribution of solutes because these processes create substantial differences in concentrations over distances of a few millimetres from root surfaces. Many rhizosphere processes are dynamic (Darrah 1993; Gregory and Hinsinger 1999; Wenzel et al. 2001; Hinsinger et al. 2006), therefore a non-destructive, non-invasive method to observe rhizosphere processes resolved in space and time is desirable.

The uptake of trace metals, such as nickel, by roots, is generally considered to occur through more or less specific membrane transporters (Zhao et al. 2002; Whiting et al. 2003). If a metal is removed by roots from the rhizosphere more rapidly than it can be re-supplied, by bulk soil via desorption and diffusion, the metal will become depleted adjacent to the root surface (Tinker and Nye 2000). In contrast, if the mass flow of a solute from the bulk soil towards the roots exceeds the uptake rate of the solute, then a concentration gradient opposing the advection flux will develop. The resulting concentration profiles are further influenced by chemical reactions with other compounds in the rhizosphere and with the soil matrix. Although these processes in rhizosphere have been discovered earlier, but due to technical limitations, they have never been observed in situ with sufficient temporal and spatial resolution. Combining new non-destructive measurement techniques such as MRI and numerical simulations can unravel some aspects of these complex interactions.

Among other new techniques, Magnetic Resonance Imaging (MRI) has been proposed to assess the spatial distribution of water and metal ions in porous media (Herrmann et al. 2002; Pierret et al. 2003; Moradi et al. 2008). The presence of paramagnetic ions and molecules in a solution affects the spin vector relaxation times (longitudinal relaxation time T_1 and transverse relaxation time T_2) of water protons (^1H). The determination of these relaxation times provides opportunities to trace the movement and diffusion of dissolved paramagnetic compounds and ions such as Ni^{2+} in the porous media. However, applying MRI to soil-plant system has several limitations. The presence of ferromagnetic particles and other paramagnetic compounds in soils can distort the MRI images and cause signal loss. Therefore, at the present state, this technique mainly is applied to carefully selected media such as pre-treated sand and soil, agar, and glass beads.

In a previous study we developed a MRI method to study the temporal and spatial distribution of dissolved Ni^{2+} ions in a porous medium under the influence of absorption by an exchange resin (Moradi et al. 2008). Here we showed that MRI can detect concentration profiles and thus can be used to investigate Ni^{2+} uptake by hyperaccumulator plants in a more complex system. We studied the two-dimensional spatial and temporal distribution of Ni^{2+} from a planar monolayer mat of roots of the hyperaccumulator plant *Berkheya coddii*. We also used numerical modelling to interpret the measurements and to analyse the dependence of the Ni^{2+} gradient adjacent to the roots on transpiration rate, uptake rate and initial concentration of Ni^{2+}.

Materials and methods

Rhizobox setup and plant growth

The rhizoboxes (inner dimensions, 100×100×30 mm) used in this study (Fig. 1) were a modified

Fig. 1 The rhizobox set up with a view of the outlet and inlet ports (*left*) and the root-only compartment (*right*)

version of the rhizobox system developed and tested by Wenzel et al. (2001). We changed the frame of the rhizobox so that the MRI receiver coils could be installed close to the root plane on the transparent side of the rhizobox (an acrylic window for root visualization and root growth control) to obtain maximal coil sensitivity in the volume of interest. We sealed the rhizoboxes using rubber bands and silicon glue. The experiment started from fully water-saturated condition, which gave the strongest MRI signal-to-noise ratio (SNR). We also redesigned the inlet and outlet ports and increased their number to 30 per box, arranged on one side of the box in five rows of six ports each, in order to improve the regulation of the nutrient solution in the main compartment of the rhizobox.

Seeds of *Berkheya coddii* were pre-germinated in perlite and grown until they were 2 weeks old. The seedlings were transferred to the upper compartment of the rhizoboxes. The main and the upper compartments of each rhizobox were filled with porous glass beads (Sera Werke, Germany) of 0.4–1.0 mm-diameter. The total porosity of the packing was 65% *v*/*v*, and the bulk density was 0.46 g cm^{-3}. Four rhizoboxes were prepared in total and four seedlings were planted per rhizobox. After transplanting, the rhizoboxes were kept for 8 weeks in a climate chamber with a daily light cycle (1.0–1.2 lumen cm^{-3}) of 16 h light/ 8 h darkness, constant humidity (75%) and controlled temperature (23/16°C day/night). The rhizoboxes were irrigated with nutrient solution (Kraemer et al. 1996). A peristaltic pump was used to circulate the nutrient solution through the rhizoboxes at a rate of around 0.6 l per day. The lower two rows of the ports were used as inlets for the nutrient solution and the ports of the uppermost row were used as outlets. Roots started to grow into the root-only compartment a week after transplanting. The root-only compartment contained no glass beads or soil. It consisted of a narrow slit separated from the glass beads by a nylon membrane with a mesh size of 20 μm. After 8 weeks of growth, one of the rhizoboxes that showed the most uniform root plane was chosen and the MRI experiments were performed on this rhizobox.

MRI technique and data analysis

MRI was performed using a Philips Intera whole-body system (Philips medical systems, Best, the Netherlands) with a static magnetic field of 1.5 Tesla that results in a proton resonance frequency of 63.8 MHz. We used a T_1 mapping technique known as variable flip angle for the quantification of T_1 (Deoni et al. 2003; Treier et al. 2007). This method calculates T_1 with the same accuracy but with a significantly shorter acquisition time than standard T_1 measurement sequences. It is based on the consecutive application of *T1*-weighted spoiled gradient-echo (*T1* fast-field echo) sequences using different flip

angles. The steady state signal achieved for a sequence using phase alternated radio-frequency (RF) pulses can be calculated using Eq. 1:

$$\frac{I(\theta)}{\sin(\theta)} = \exp(-TR/T_1)\frac{I(\theta)}{\tan(\theta)} + N(H) \times (1 - \exp(-TR/T_1)) \times \exp(-TE/T_2{}^*), \quad (1)$$

where I is the signal intensity, $N(H)$ is the proton density, θ is the RF pulse flip angle, TE is the echo time, and $T_2{}^*$ is the effective transverse relaxation time. According to Eq. 1, a plot of $I(\theta)/sin(\theta)$ vs. $I(\theta)/tan(\theta)$ should yield a straight line with slope $\exp(-TR/T_1)$. Since this slope depends only on TR, the known repetition time, one can calculate T_1 without prior knowledge of $N(H)$ or $T_2{}^*$. The effect of transverse relaxation was considered negligible for a fairly short echo times. We used an echo time of 4.5 ms, a repetition time of 9 ms, slice thickness of 15 mm, a data matrix of 512×512 pixels, and a field of view of 110×110 mm. The acquisition bandwidth was 564.10 Hz. For T_1 calculation, we cropped the image part related to the rhizobox in the middle of the original MRI matrix, therefore the images shown here are only the cross-sections of the rhizobox. We fitted the Eq. 1 to the MRI data for different flip angles and calculated the T_1 for each pixel. Due to the limited spatial sensitivity of the receiver coil, the SNR deteriorated on the two sides of the rhizobox due to the higher distance from the coil centre. To avoid measurement errors due to partial volume effects we excluded a margin of 5 mm width from the two sides of the MRI images for further analysis (Fig. 3b). A median filter with dimensions of 3×3 pixels was applied to the T_1 images to reduce noise. All the images were processed using Matlab.

In a separate experiment, we found a linear relationship between the longitudinal relaxation time, T_1, and the Ni^{2+} concentrations in glass beads saturated with Ni^{2+} solution in the concentration range of 1–30 mg l^{-1} (Fig. 2). This calibration curve was used for calculating Ni^{2+} concentrations for each pixel from the corresponding T_1 values.

Ni^{2+} uptake experiment

For the Ni^{2+} uptake experiment, the main compartment of the rhizobox was washed with eight pore-

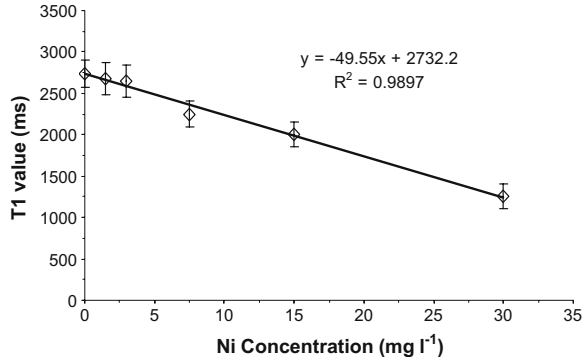

Fig. 2 The calibration of T_1 versus Ni^{2+} concentration; bars represent standard deviations of the mean

volumes of Ni^{2+} solution with a concentration of 10 mg l^{-1} (prepared using Ni $(NO_3)_2$, $6H_2O$) to replace the nutrient solution. We used the lower ports as inlets for ingoing Ni^{2+} solution and let the solution overflow over the lateral walls of the rhizobox to ensure homogeneous initial Ni^{2+} distribution in the system. This rather high concentration of Ni^{2+} was used to stay clearly above the detection limit for Ni^{2+} of 1 mg l^{-1}. The rhizobox was put into the MRI scanner (Fig. 3a) and a circular RF coil was installed on the root-plane side of the rhizobox close to the roots. The first T_1 measurement could be carried out 3 h after the Ni^{2+} solution was applied to the rhizobox. The second and the third measurement were performed 5 and 11 h after the application of Ni^{2+} solution, respectively. The amount of transpiration was measured by weighing the rhizobox before and after the experiment. We kept the upper compartment dry for a week before the MRI experiment started, therefore, evaporation during the experiment and the transpiration from the upper compartment was considered negligible and the water was assumed to be taken up by plant roots only from the main compartment of the rhizobox.

Modelling

Simulations were carried out using the numerical code MIN3P (Mayer et al. 2002), which describes variably-saturated flow and transport in three-dimensional porous media and geochemical reactions including kinetic and equilibrium mass exchange with mineral phases and roots. The simulation of variably saturated water flow is described by the Richards equation,

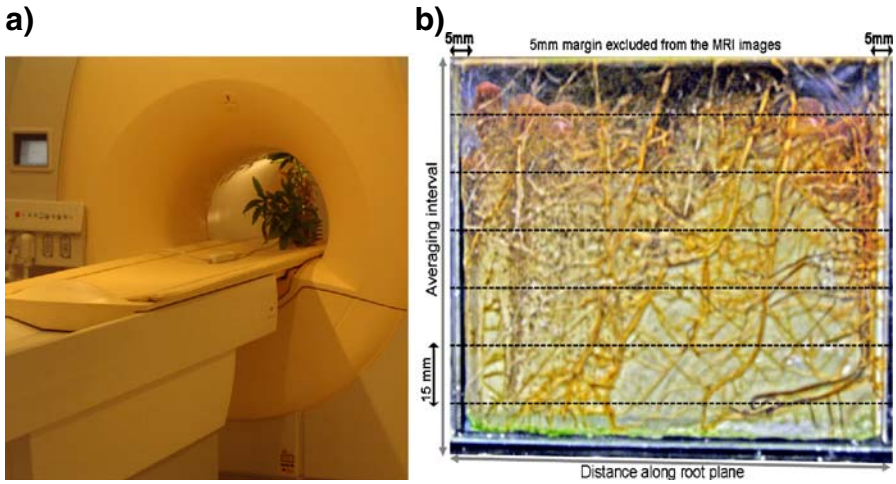

Fig. 3 A view of the rhizobox placed inside the MRI machine (**a**) and the root distribution pattern before the Ni^{2+} uptake experiment (**b**). The broken lines indicate the 15 mm thick slices into which MRI signal was recorded

which is implemented in MIN3P using the formulation (Mayer et al. 2002):

$$S_a S_s \frac{\partial h}{\partial t} + \phi \frac{\partial S_a}{\partial t} - \nabla.[k_{ra} K \nabla h] - Q_a = 0, \quad (2)$$

Where t is time (s), ϕ is the total porosity, S_a is water saturation, S_s is the specific storage coefficient (m^{-1}), Q_a is the sink/source term, K is the hydraulic conductivity tensor (m s^{-1}), k_{ra} is the relative permeability of the porous medium with respect to the aqueous phase and is related to the hydraulic head, h, and water saturation, S_a, through the standard soil hydraulic functions given by Wosten and Vangenuchten (1988).

The mass balance equation for the reactive transport of the solutes was as followings:

$$\frac{\partial}{\partial t}\left(S_a \phi T_j^a\right) = \nabla.\left(S_a \phi D_a \nabla T_j^a\right) - \nabla.\left(\nu T_j^a\right) - R_j - q T_j^a, \quad (3)$$

Where T_j^a is the total aqueous concentration of the component j (mol m^{-3}), ν is the Darcy velocity (m s^{-1}), D_a is the hydrodynamic dispersion coefficient (m^2 s^{-1}), Rj is the sink/source term for kinetically-controlled reactions, and q is the water uptake flux (s^{-1}).

We used MIN3P to simulate Ni^{2+} distribution in the rhizobox and adjacent to the root plane as being taken up by roots. The simulation was set to start with the initial condition of water saturated for the rhizobox and no flux from the boundaries except for the root plane that was assumed to be a homogeneous sink for water and Ni^{2+} Soil hydraulic function parameters were set to following values; residual water content was 0.05, Van Genuchten α was 0.143 m^{-1}, Van Genuchten n was 1.506 and Van Genuchten l was 0.65. Water was set to be taken up at a constant rate during the experiment. Nickel uptake was modeled following the approach by Lombi et al. (2001) that adds a linear component to the Michaelis-Menten kinetics:

$$F_M = \frac{k_m c}{K_m + c} + \alpha c, \quad (4)$$

where F_M is the root uptake rate per unit surface of the roots (mol m^{-2} s^{-1}), k_m is the effective rate coefficient (mol m^{-2} s^{-1}), K_m is the Michaelis-Menten's constant (mol m^{-3}), c is the Ni^{2+} concentration in solution (mol m^{-3}), and α is the slope of the linear component (mol m^{-2} s^{-1}).

Sensitivity analysis showed that the most critical parameters were uptake rate coefficient and transpiration rate (data not shown here). The Ni^{2+} uptake rate coefficient, the Michaelis-Menten's constant and the linear component were varied randomly to yield the observed temporal evolution of the Ni^{2+} distribution. Root mean square error (RMSE) measure was used to evaluate the simulations and the one with the smallest RMSE was finally chosen. The Ni^{2+} diffusion coefficient in free aqueous solution was set to 1.25×10^{-9} m^2 s^{-1}. The dispersivity was set to 9.0×10^{-4} m,

which reflects the grain-size of the glass beads we used (0.4–1.0 mm) and agrees with the typical range of dispersivity in soils (Aggelopoulos and Tsakiroglou 2007). The initial Ni^{2+} concentration was 10 mg l^{-1}. The other parameters were taken directly from the experiment. The glass beads were chemically inert; therefore, no sorption isotherm was used. The grid resolution for numerical solution was set to correspond to the spatial resolution of the MRI measurement, except that a finer grid was chosen in the direct vicinity of the roots for better convergence with the numerical solution.

Results

Temporal changes of Ni^{2+} distribution

Figure 3b shows the distribution pattern of roots in the root-only compartment before the Ni^{2+} uptake experiment started. The horizontal sections, separated by the dashed lines correspond to the slices into which the MRI signals were collected. There was a dense layer of roots in the first two slices, but the root density was lower in the bottom of the rhizobox. The root mat was composed of old and young roots in all slices. The root distribution was most homogeneous in the 3rd, 4th and 5th slice from the top. These three slices remained water saturated during the course of experiment, therefore, they were chosen for calculations of T_1 and Ni^{2+} concentration profiles.

The Ni^{2+} distribution maps measured at various times after the application of Ni^{2+} solution are shown in Fig. 4. Each Ni^{2+} distribution map represents a pixel-wise average value of the slices 3, 4 and 5 that were calculated from the corresponding T_1 values using the calibration curve in Fig. 2. T_1 values ranged from 1,800 ms near the root plane to slightly above 2,400 ms in the corners of the rhizobox farthest away from the root plane (data not shown here). Compared to the middle of the rhizobox, the corners of the rhizobox were farthest away from the coil centre and showed a weaker SNR and therefore considerably higher variability in the calculated T1 and the corresponding Ni^{2+} concentrations. This indicates that the reliability of the measurement decreased with distance from the coil centre due to a decline in SNR. Already at the first measurement, 3 h after the start of

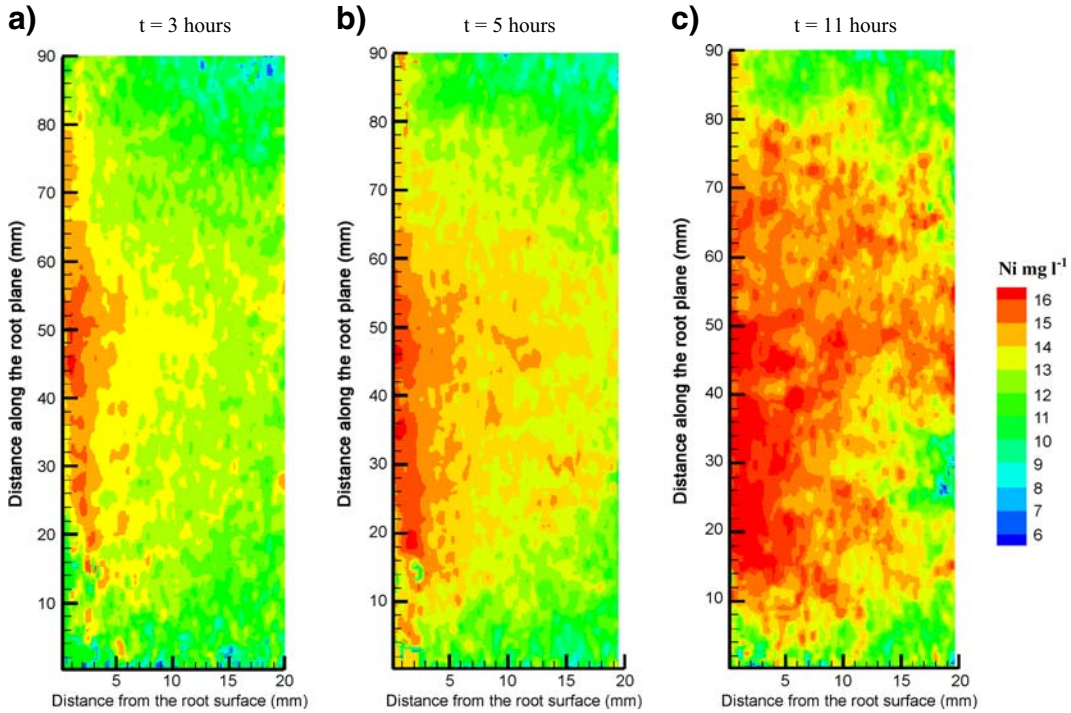

Fig. 4 Horizontal two-dimensional maps of Ni^{2+} distribution in the root zone of Berkheya coddii 3 h (**a**), 5 h (**b**), and 11 h (**c**) after Ni^{2+} application to the rhizobox

the experiment (application of Ni^{2+} solution to the rhizobox), a gradient in the Ni^{2+} concentration was visible (Fig. 4a). The Ni^{2+} concentration ranged from around 15 mg l^{-1} immediately adjacent to the root-plane to slightly above 10 mg l^{-1} at a distance of 20 mm away from the roots on the opposite side of the rhizobox. This indicates that the amount of Ni^{2+} transported to the root surface via convection was greater than the amount of Ni^{2+} taken up by the roots. The roots partially excluded the Ni^{2+} and the extent of the exclusion in the middle of the root-plane was greater than at the edges. This variability might be related to the inhomogeneous distribution and activity of the roots. After 5 h, the Ni^{2+} accumulation zone extended to a distance of more than 20 mm away from the root surface in the middle of the root-plane (Fig. 4b). The Ni^{2+} accumulation zone extended to the sides of the rhizobox 11 h after the experiment had started (Fig. 4c), while the magnitude of the accumulation was still highest in the middle.

Ni^{2+} concentration mapping at different soil water contents

As the plants transpired water, the water level in the rhizobox dropped and the upper part of the rhizobox became unsaturated. With the decrease in water content, also the SNR decreased in the upper part of the rhizobox (mainly first and the second slice from top). This resulted in high variability in the calculated T_1 values. T_1 maps of horizontal cross-sections through the rhizobox at the upper first slice (unsaturated), the second slice (partly saturated), and the 4th slice (saturated) are shown in Fig. 5a, b, and c, respectively. In the unsaturated zone (Fig. 5a), the SNR was much poorer than in the saturated zone below. Water was the main signal-bearing source in our system, therefore a decrease in water content resulted in decrease in SNR. Since the main aim here was to visualize Ni^{2+} concentrations close to the roots where full water saturation was persistent during the experiments, we did not further process the MRI data from the unsaturated part of the rhizobox. The SNR increased in the second slice of the rhizobox in the transition zone between saturated and unsaturated zone (Fig. 5b) i.e. in the zone of capillary fringe above the water level, but the signal was considerably lower and more heterogeneous than in the fully saturated zone (Fig. 5c).

Modelling Ni^{2+} uptake

Figure 6 shows the MRI-measured and the simulated average profiles of Ni^{2+} concentrations with distance from the root plane for each measurement time. The MRI-measured averages were taken column-wise parallel to the root plane from the 3rd, 4th, and 5th slices.

The best agreement between the simulated and MRI-measured Ni^{2+} concentration profiles (based on RMSE analysis) was obtained when the uptake rate coefficient was set to 1.17×10^{-8} mol m^{-2} s^{-1}, the Michaelis-Menten's constant to 2.5×10^{-4} mol m^{-3}, and the linear component to 1.05×10^{-9} mol m^{-2} s^{-1}. These values are well in the same order of magnitude with the published rates for zinc and cadmium by other hyperaccumulator plants (Lombi et al. 2001; Zhao et al. 2006). The concentration range of Ni^{2+} in solution was almost three orders of magnitude higher than the optimized Michaelis-Menten's constant which shows that the Ni^{2+} uptake by root was mainly passive instead of active. The simulation of the averaged Ni^{2+} profile at t=3 h was the most satisfactory (RMSE=0.20 compared to 0.26 and 0.46 for t=5 and 11 respectively). The MRI-measured Ni^{2+} concentration was in good agreement with the simulated Ni^{2+} profile over the whole length from the root plane to the opposite wall. For t=5 and 11, the simulated Ni^{2+} concentration profiles were slightly overestimated adjacent to the root surface and underestimated at farther distances namely 5–15 mm from the roots. The MRI-measured Ni^{2+} profiles showed a gentler slope than the simulated ones.

Effects of various parameters on Ni^{2+} concentration profile

The magnitude and the sign of the Ni^{2+} gradient adjacent to the roots are essentially a function of Ni^{2+} concentration in solution, the rate of Ni^{2+} uptake by the roots, and the transpiration rate. We performed a sensitivity analysis by varying each one of these parameters at a time while keeping the other parameters constant. Figure 7 shows how transpiration rate affected the simulated Ni^{2+} concentration gradient. The transpiration rate was reduced by 45 and 85%, while all other parameters were kept constant. Reduction of the transpiration by 45% eliminated the gradient profile, while 85% reduction in transpi-

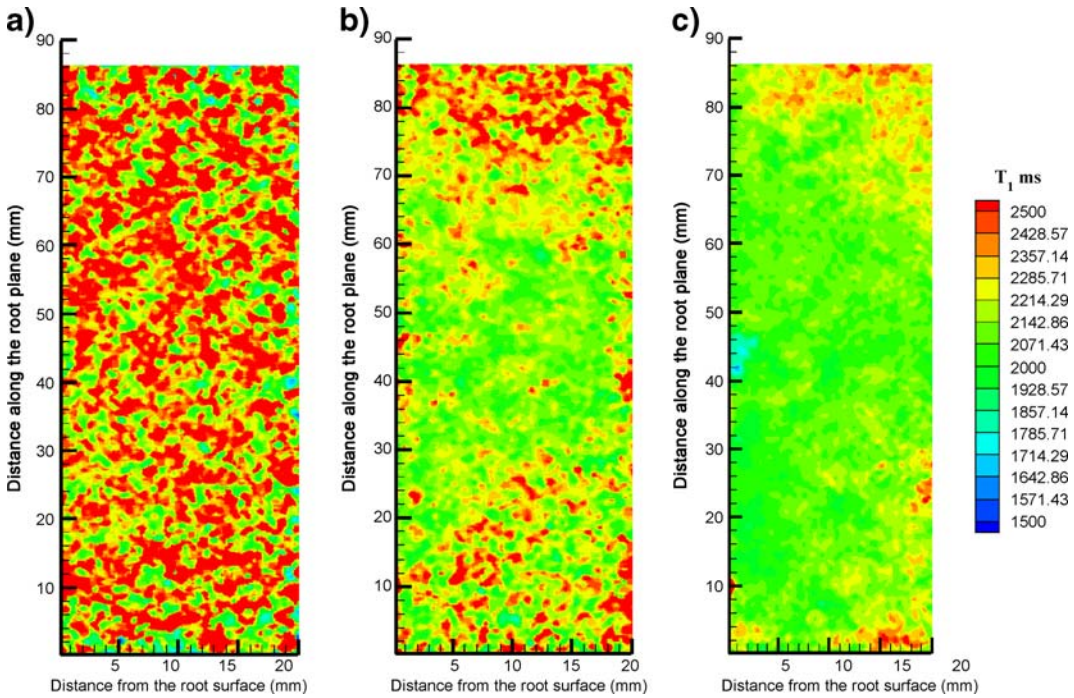

Fig. 5 T_1 maps at horizontal cross-sections of the rhizobox at t=11 h when the water level dropped in the rhizobox: **a**) 1st slice from top where it was unsaturated, **b**) 2nd slice partly saturated, and **c**) 4th slice completely saturated

ration resulted in a negative gradient towards the roots.

Varying the uptake rate coefficient had similar effects on the Ni^{2+} concentration profile (Fig. 8). The Ni^{2+} concentration gradient became gentler and then disappeared when the uptake rate coefficient was increased to 2.7×10^{-8} and 4.95×10^{-7} mol m^{-2} s^{-1} respectively. Using an uptake rate coefficient of 1.62×10^{-6} mol m^{-2} s^{-1} resulted in Ni^{2+} depletion in the rhizosphere.

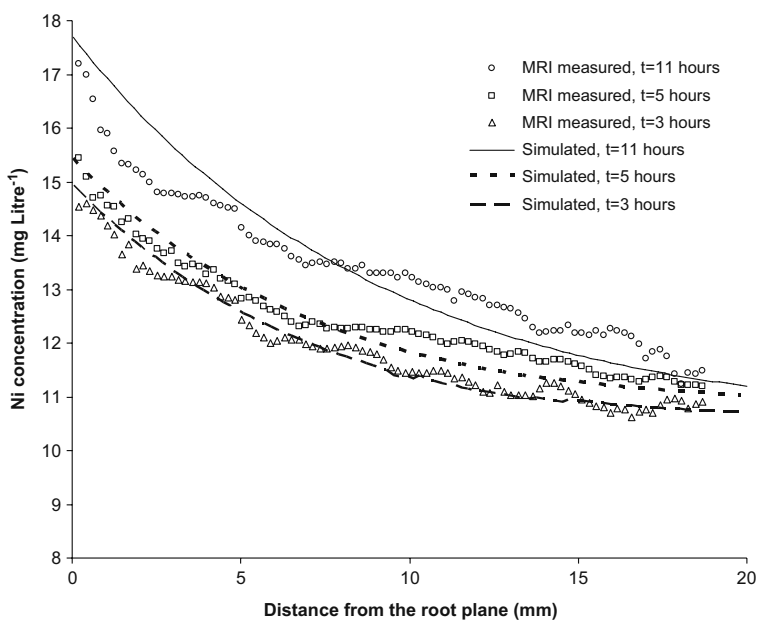

Fig. 6 The MRI-measured and simulated Ni^{2+} concentration profiles as a function of distance from the root plane at 3, 5, and 11 h after Ni^{2+} application. The Ni^{2+} uptake rate coefficient was set to 1.17×10^{-8} mol m^{-2} s^{-1}

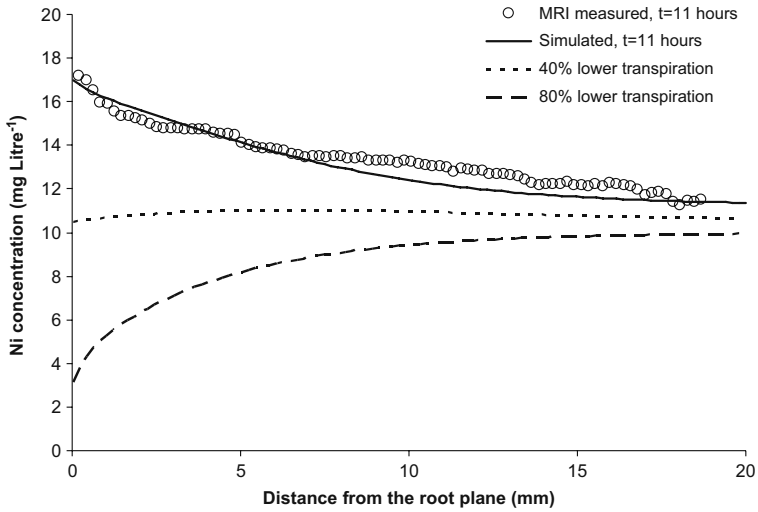

Fig. 7 The MRI-measured and simulated Ni^{2+} concentration profile as a function of distance from root surface at t=11 h and the simulation results assuming a transpiration rate of 45 and 85% of the measured transpiration for *Berkheya coddii*

Figure 9 shows simulated Ni^{2+} gradients assuming various initial concentration of Ni^{2+} in soil solution. The Ni^{2+} gradients were normalized by dividing by the initial Ni^{2+} concentrations. Using the same input parameters but varying the initial concentration of Ni^{2+}, resulted in different Ni^{2+} gradients. For Ni^{2+} initial concentration of 1 mg l^{-1}, the simulated accumulation pattern was gentler than 10 mg l^{-1}. A slight Ni^{2+} depletion was obtained for Ni^{2+} initial concentration of 0.1 mg l^{-1} while assuming a Ni^{2+} initial concentration of 0.01 mg l^{-1} resulted in an exhaustion of Ni^{2+} in the soil solution in the rhizosphere.

Discussion

The experimental set-up that we used here is a compromise between a MRI-suited medium and a realistic soil-root system. Nevertheless, MRI proved to be useful to study the dynamics of Ni^{2+} in the vicinity of the roots of hyperaccumulator plants non-destructively. Here for the first time we obtained Ni^{2+} concentration maps in the root zone of *Berkheya coddii* with spatial resolution of 0.21 mm and temporal resolution of only minutes. There is a gap of knowledge about the uptake behaviour of hyperaccumulator plants. There is also

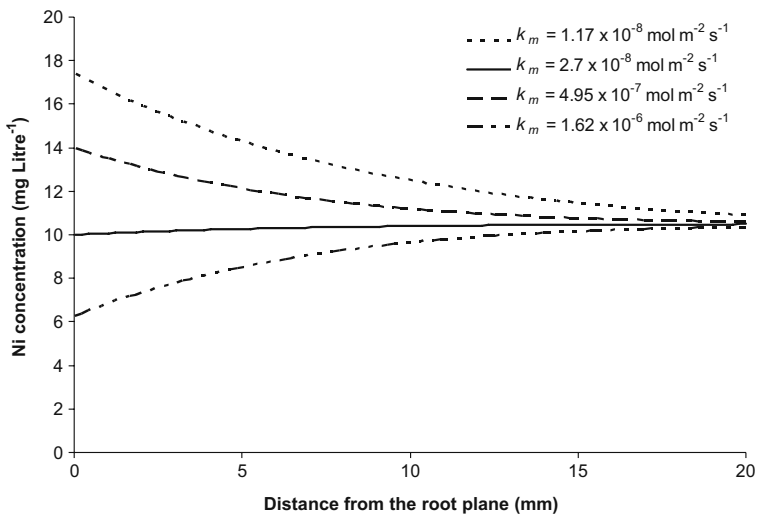

Fig. 8 Simulated Ni^{2+} concentration profiles as a function of distance from root surface for four different uptake rate coefficients. All other parameters were kept constant

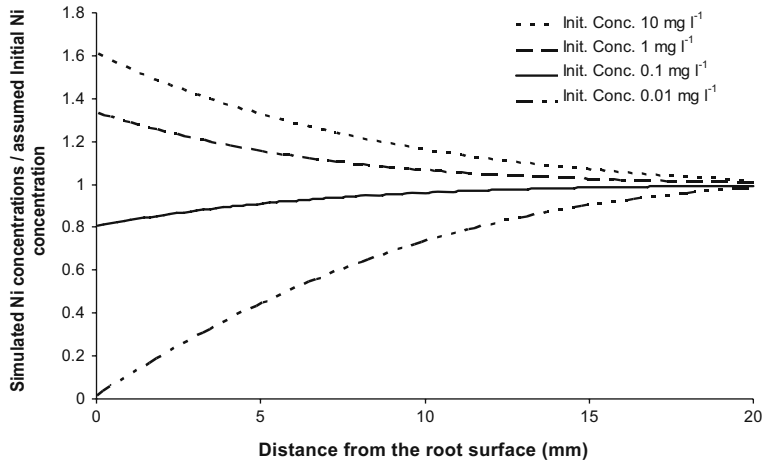

Fig. 9 Simulated Ni^{2+} concentration profile as a function of distance from root surface assuming various initial concentrations. Ni^{2+} concentration profiles were normalized by dividing by the corresponding initial concentration. All other parameters were kept constant

desire for a non-destructive non-invasive technique to study rhizosphere processes. Therefore, MRI can be used to study the uptake behaviour of hyperaccumulator plants. However there are several limitations in applying MRI to a real soil-root system. The porous medium that was used here is chemically inert, while the real soil-root system requires accounting for interactions between the ions in the soil solution and the solid phase. MRI was proved to suffer from fading of SNR in unsaturated conditions. The resulting SNR from the unsaturated zone of the rhizobox showed a considerable degree of random variability in unsaturated conditions, representing variations of water content but also water distribution in the pore space. Our images had a spatial resolution of 0.21×0.21 mm, a slice thickness of 15 mm, and therefore, a voxel size of 0.21×0.21× 15 mm. Considering the size of the glass beads (0.4–1.0 mm), the voxel's space was occupied by a random combination of beads and pore space that affects the relaxation behaviour and SNR. This holds true for even a completely water-saturated porous medium. Since each voxel contains a specific combination of beads, pore space and water content, it returns a specific SNR, which is different from the neighbouring voxels. This could be an advantage or disadvantage depending on the type of the information that is desired. For example, it clearly reflects the heterogeneity of the system. However, it makes any averaging of the MRI signal, T_1 or concentrations along a profile deviating. Therefore, the voxel size should be optimised based on the aims of the study. Additionally, the variability of water saturation of the intra-grain pore space might affect the T_1 relaxation behaviour and SNR (Fig. 5). To correct for this, separate calibration curves would be needed for given water contents and possibly also for different water distribution patterns in the pore space. Another shortcoming is the detection limit of MRI for Ni^{2+} concentration. We could resolve Ni^{2+} concentrations down to 1 mg l^{-1}. However, this could be improved at the cost of measurement time and spatial resolution.

The increase in Ni^{2+} concentration towards the root surface (Fig. 4) means that Ni^{2+} uptake by roots was not limited by diffusion at these relatively high soluble Ni^{2+} concentrations. Our result suggests that *Berkheya coddii* can hyperaccumulate Ni in soils with high Ni concentration in soil solution without actively solubilizing Ni in the root zone. Therefore, the Ni diffusion in such soils is not the limiting factor for phytoremediation or phytomining purposes. This might be the case in serpentine soils, where *Berkheya coddii* is native.

Our simulation results showed that metal concentration gradient in the rhizosphere is very dynamic and is controlled by plant's transpiration rate, metal uptake rate and the metal concentration in the soil solution (Figs. 7, 8, and 9). Diurnal change of transpiration is expected to affect the gradients of metals in the rhizosphere. For example for metals and ions that are abundant in soil solution, a positive gradient might develop at the peak of transpiration rate in midday, while it may disappear by reduction in transpiration in the evenings. Metal gradients in the rhizosphere of various plant species with various uptake properties might be different. Plants with

lower metal uptake-rate are more likely to experience accumulation of metal near their roots.

The total Nickel extractable by 1 *M* ammonium acetate was found to reach concentrations up to 12 mg l^{-1} in serpentine soils in *Berkheya coddii*'s native environment (Robinson et al. 1997), while it is usually present in much lower concentrations in other soils. The metal concentration profile in the rhizosphere of the plants growing in highly contaminated soils might differ from those in less contaminated soils. Figure 9 illustrates that an initial concentration of 10 mg l^{-1} resulted in an accumulation pattern, while an initial concentration of less than 0.1 mg l^{-1} resulted in an extensive depletion of Ni^{2+} adjacent to the roots. This shows that a depletion of Ni^{2+} is expected at low dissolved concentrations of Ni^{2+} in soil solution, if the uptake rate stays unchanged. However, the interactions between the sorbed and soluble Ni in soil needs to be considered. Puschenreiter et al. (2005) studied Ni in the rhizosphere of the hyperaccumulator *Thlaspi goesingense* and reported an accumulation of Ni in soil solution at the root surface but a depletion of labile Ni towards the roots. Their results suggests that hyperaccumulation of Ni (at much lower Ni concentrations in soil solution than in our case) is influenced by the interactions between Ni in soil solution and the soil solid-phase. They also highlighted the importance of root-induced changes in the rhizosphere. Local changes in dissolved organic matter and pH due to root exudates can influence the speciation of metals in the soil solution and their mobilisation from the soil solid-phase. These interactions were not accounted for here, neither in the MRI measurements nor in the modelling.

In conclusion, this study shows that even though the real soil-root system was to some extent compromised, combination of MRI and numerical modelling could provide some valuable insight into the dynamic of metals in the root-soil interface. Ni uptake by *Berkheya coddii* was shown to be passive and Ni was partly excluded from the roots and accumulated in the rhizosphere at the concentration range that was used here. The accumulation or depletion of Ni^{2+} in the root zone of hyperaccumulator plants were demonstrated to be a delicate function of sensitive parameters such as transpiration rate, Ni^{2+} uptake rate and initial Ni^{2+} concentration in the soil solution. Our simulation results showed that while decreasing the Ni^{2+} uptake rate coefficient resulted in accumulation of Ni^{2+} in the rhizosphere, a depletion pattern was developed when the initial Ni^{2+} or the transpiration rate was reduced.

Acknowledgements This study was funded by the Swiss National Science Foundation. We would like to thank Reto Treier (IBE, ETH Zurich) for his technical support on T_1 calculations.

References

Aggelopoulos CA, Tsakiroglou CD (2007) The longitudinal dispersion coefficient of soils as related to the variability of local permeability. Water Air Soil Poll 185:223–237

Ashworth DJ, Alloway BJ (2004) Soil mobility of sewage sludge-derived dissolved organic matter, copper, nickel and zinc. Environ Pollut 127:137–144

Brooks RR (ed) (1998) Plants that hyperaccumulate heavy metals. CAB International, Wallingford

Brooks RR, Lee J, Reeves RD, Jaffre T (1977) Detection of nickeliferous rocks by analysis of herbarium specimens of indicator plants. J Geochem Explor 7:49–57

Brooks RR, Chambers MF, Nicks LJ, Robinson BH (1998) Phytomining. Trends Plant Sci 3:359–362

Darrah PR (1993) The rhizosphere and plant nutrition—a quantitative approach. Plant Soil 156:1–20

Deoni SCL, Rutt BK, Peters TM (2003) Rapid combined T-1 and T-2 mapping using gradient recalled acquisition in the steady state. Magn Reson Med 49:515–526

Gregory PJ, Hinsinger P (1999) New approaches to studying chemical and physical changes in the rhizosphere: an overview. Plant Soil 211:1–9

Herrmann KH, Pohlmeier A, Wiese S, Shah NJ, Nitzsche O, Vereecken H (2002) Three-dimensional nickel ion transport through porous media using magnetic resonance imaging. J Environ Qual 31:506–514

Hinsinger P, Plassard C, Jaillard B (2006) Rhizosphere: a new frontier for soil biogeochemistry. J Geochem Explor 88:210–213

Kraemer U, CotterHowells JD, Charnock JM, Baker AJM, Smith JAC (1996) Free histidine as a metal chelator in plants that accumulate nickel. Nature 379:635–638

Li YM, Chaney R, Brewer E, Roseberg R, Angle JS, Baker A, Reeves R, Nelkin J (2003) Development of a technology for commercial phytoextraction of nickel: economic and technical considerations. Plant Soil 249:107–115

Lombi E, Zhao FJ, McGrath SP, Young SD, Sacchi GA (2001) Physiological evidence for a high-affinity cadmium transporter highly expressed in a *Thlaspi caerulescens* ecotype. New Phytol 149:53–60

Mayer KU, Frind EO, Blowes DW (2002) Multicomponent reactive transport modeling in variably saturated porous media using a generalized formulation for kinetically controlled reactions. Water Resour Res 38:1174–1194

McNear DH, Peltier E, Everhart J, Chaney RL, Sutton S, Newville M, Rivers M, Sparks DL (2005) Application of quantitative fluorescence and absorption-edge computed microtomography to image metal compartmentalization in Alyssum murale. Environ Sci Technol 39:2210–2218

Moradi AB, Oswald SE, Massner JA, Pruessmann KP, Robinson BH, Schulin R (2008) Magnetic Resonance Imaging methods to reveal the real-time distribution of nickel in porous media. Eur J Soil Sci 59:476–485

Pierret A, Doussan C, Garrigues E, Mc Kirby J (2003) Observing plant roots in their environment: current imaging options and specific contribution of two-dimensional approaches. Agronomie 23:471–479

Puschenreiter M, Schnepf A, Millan IM, Fitz WJ, Horak O, Klepp J, Schrefl T, Lombi E, Wenzel WW (2005) Changes of Ni biogeochemistry in the rhizosphere of the hyperaccumulator *Thlaspi goesingense*. Plant Soil 271:205–218

Robinson BH, Brooks RR, Howes AW, Kirkman JH, Gregg PEH (1997) The potential of the high-biomass nickel hyperaccumulator *Berkheya coddii* for phytoremediation and phytomining. J Geochem Explor 60:115–126

Robinson BH, Brooks RR, Gregg PEH, Kirkman JH (1999) The nickel phytoextraction potential of some ultramafic soils as determined by sequential extraction. Geoderma 87:293–304

Tinker PB, Nye PH (2000) Solute movement in the rhizosphere. Oxford University Press, New York

Treier R, Steingoetter A, Fried M, Schwizer W, Boesiger P (2007) Optimized and combined T-1 and B-1 mapping technique for fast and accurate T-1 quantification in contrast-enhanced abdominal MRI. Magn Reson Med 57:568–576

Wenzel WW (2005) Rhizosphere conference. J Environ Qual 34:2156–2156

Wenzel WW, Wieshammer G, Fitz WJ, Puschenreiter M (2001) Novel rhizobox design to assess rhizosphere characteristics at high spatial resolution. Plant Soil 237:37–45

Whiting SN, Broadley MR, White PJ (2003) Applying a solute transfer model to phytoextraction: zinc acquisition by *Thlaspi caerulescens*. Plant Soil 249:45–56

Wosten JHM, Vangenuchten MT (1988) Using texture and other soil properties to predict the unsaturated soil hydraulic functions. Soil Sci Soc Am J 52:1762–1770

Zhao FJ, Hamon RE, Lombi E, McLaughlin MJ, McGrath SP (2002) Characteristics of cadmium uptake in two contrasting ecotypes of the hyperaccumulator *Thlaspi caerulescens*. J Exp Bot 53:535–543

Zhao FJ, Jiang RF, Dunham SJ, McGrath SP (2006) Cadmium uptake, translocation and tolerance in the hyperaccumulator Arabidopsis halleri. New Phytol 172:646–654